Journal of ELECTRONIC MATERIALS, Vol. 44, No. 11, 2015
DOI: 10.1007/s11664-015-3977-0

Optimization of the Mechanical and Electrical Performance of a Thermoelectric Module

ALI SARHADI,[1,2] RASMUS BJØRK,[1] and NINI PRYDS[1]

1.—Department of Energy Conversion and Storage, Technical University of Denmark, 4000 Roskilde, Denmark. 2.—e-mail: asar@dtu.dk

Finite-element simulation of a thermoelectric (TE) module was conducted to optimize its geometrical dimensions in terms of mechanical reliability and performance. The TE module consisted of bismuth telluride *n*- and *p*-type legs. The geometrical dimensions of the module, i.e., leg length and leg cross-sectional area, were varied, and the corresponding maximum thermal stress, output power, and efficiency of the module obtained. An optimal design for the module was then suggested based on minimizing the thermal stresses and maximizing the performance, i.e., power and efficiency. The optimal dimensions at maximum von Mises stress of 75 MPa were leg length of 2 mm to 2.5 mm and leg width of 1.5 mm to 2 mm, resulting in efficiency of 7.2%. Finally, the influence of solders, i.e., solder material between the leg, the interconnector, and the top ceramic layer, on the induced thermal stresses and module performance was investigated. The results revealed that the transition from elastic to plastic deformation in the solder decreased the induced thermal stresses significantly. Moreover, beyond the elastic limit, the stress magnitude was highly dependent on the magnitude and mechanism of plastic deformation in the module. The present study provides a basis for a unique and new optimization scheme for TE modules in terms of endurance and performance.

Key words: Thermoelectric, thermomechanical modeling, design optimization, efficiency, output power

INTRODUCTION

Application of thermoelectric (TE) modules in innovative energy technologies necessitates greater attention to optimal design of these modules to enhance their lifetime and efficiency under operating conditions. Design optimization of TE modules can be performed for two objectives, namely mechanical strength and functional performance, i.e., efficiency and/or output power.[1] Module design for mechanical strength mainly focuses on the induced internal thermal stresses, as the thermal expansion mismatch between different materials in a thermoelectric module can cause its failure. Evaluating the thermally induced stresses in TE modules has therefore been the subject of several research works; Suhir and Shakouri developed a one-dimensional analytical elastic model to calculate the interfacial thermal shear stress in a TE module, taking into account free boundary conditions.[2,3] Based on their calculations, they concluded that using thin and long legs reduces the interfacial shear stresses, hence increasing the mechanical reliability of the modules. Moreover, it was shown that the maximum value of the shear stress occurred at the edges of the legs.[4] Similar results were also obtained by Clin et al.[5] Growth of thermal stresses in TE modules when selecting short and thick legs has also been reported by other researchers.[6] Moreover, thermomechanical modeling of segmented TE modules has shown that selecting appropriate soldering alloy can reduce the induced thermal stresses in the modules through stress relaxation in the soldering alloy when undergoing plastic deformation.[7] Most of

(Received October 11, 2014; accepted August 9, 2015; published online August 26, 2015)

these cited works focused only on thermomechanical modeling of TE modules, considering some simplifying assumptions such as elastic material models. Despite this, thermomechanical modeling of a TE module provides an efficient tool for assessing the mechanical strength of the modules and subsequently optimizing it in terms of the mechanical reliability, but designing a TE module only in terms of mechanical reliability is not enough, as the efficiency must also be considered. These two objectives may however conflict with each other, and improvement of one may deteriorate the other. Therefore, one must investigate whether there is an inherent tradeoff between mechanical reliability and module efficiency and subsequently optimize the TE module taking into account these two objectives, which so far has not been addressed in the literature.

Thus, the current study deals with finite-element (FE) simulations of a TE module with the aim of optimizing the geometrical dimensions in terms of mechanical reliability as well as functional efficiency. FE simulations of a module consisting of 2×2 legs of p- and n-type bismuth telluride, respectively, were carried out. The geometrical dimensions of the module were varied, and the corresponding thermal stresses, output power, and efficiency calculated. Based on these results, proper geometrical dimensions for the TE legs are suggested. Finally, the effect of the solder and interconnector materials on the thermal stresses in the module is investigated.

THEORY OF ELASTOPLASTIC MATERIALS

To correctly model the thermomechanical behavior of a TE module, one cannot only assume linear elastic behavior of the different components, as the thermally induced stresses are too high. Instead, elastoplastic material behavior must be assumed. The stress–strain behavior of an elastoplastic material can be characterized as an elastic region until yielding commences at a yielding stress of σ_Y, followed by a plastic region. In the elastic region, the stress–strain relation in the presence of a thermal gradient has a linear form (Hooke's law):

$$\sigma = C : \underbrace{\left(\varepsilon - \varepsilon^{th}\right)}_{\varepsilon^e}, \tag{1}$$

where C, σ, ε, and $\varepsilon^{\mathrm{th}}$ are the fourth-order elasticity tensor, Cauchy stress tensor, and total and thermal strain tensors, respectively.

In the plastic region, assuming that the plastic deformation is rate independent, the incremental form of the stress–strain relation is given by[8]

$$\mathrm{d}\sigma = C : \underbrace{\left(\mathrm{d}\varepsilon - \mathrm{d}\varepsilon^{p} - \mathrm{d}\varepsilon^{th}\right)}_{\mathrm{d}\varepsilon^{e}.} \tag{2}$$

The increment of the plastic strain tensor $\mathrm{d}\varepsilon^{p}$ is defined by the flow rule[9]

$$\mathrm{d}\varepsilon_{ij}^{\mathrm{p}} = \mathrm{d}\lambda \frac{\partial Q_{\mathrm{p}}}{\partial \sigma_{ij}}, \tag{3}$$

where $\mathrm{d}\lambda$ is a proportional positive scalar multiplier which depends on the current state of the stress and load history. Q_{p} is the plastic potential, where $Q_{\mathrm{p}}(\sigma_{ij}) = d$ or constant, represents a surface in the six-dimensional stress state where the plastic strain $\mathrm{d}\varepsilon_{ij}^{\mathrm{p}}$ can be represented as a vector perpendicular to this surface. For metals, it can be assumed that the plastic potential function Q_{p} is the same as the yield function F_{y} (associated flow rule). Experimental observations show that the associated flow rule represents the plastic deformation of metals quite well.[9] Therefore, the associated flow rule is given by

$$\mathrm{d}\varepsilon_{ij}^{\mathrm{p}} = \mathrm{d}\lambda \frac{\partial F_{\mathrm{y}}}{\partial \sigma_{ij}}, \tag{4}$$

where F_{y} can be expressed as

$$F_{\mathrm{y}} = \emptyset(\sigma) - \sigma_{\mathrm{y}}(\kappa), \tag{5}$$

where $\emptyset(\sigma)$ is the effective stress, which can be expressed in the form of the von Mises stress, Tresca stress, and other user-defined functions. The von Mises stress is widely used in metal plasticity.[8] σ_{y} is the yield stress, which can be determined by a hardening rule, and κ is the hardening parameter, which can be related to the effective plastic strain as

$$\kappa = \bar{\varepsilon}_{\mathrm{p}}. \tag{6}$$

The effective plastic strain is defined as

$$\mathrm{d}\bar{\varepsilon}_{\mathrm{p}} = \sqrt{\frac{2}{3}(\mathrm{d}\varepsilon_{ij}^{\mathrm{p}})(\mathrm{d}\varepsilon_{ij}^{\mathrm{p}})}. \tag{7}$$

After the initial yielding, the subsequent plastic deformation may be dependent on the current plastic strain. This phenomenon is called strain hardening. Isotropic and kinematic strain hardening are two major models that are used for elastoplastic materials. If subsequent yield surfaces expand uniformly without translation, the hardening model is said to be isotropic. On the other hand, if the subsequent yield surfaces preserve their shape and orientation, but translate in the stress space, the hardening model is kinematic.[9,10]

In the case of an isotropic hardening model, the yield stress in Eq. 4 depends on the effective plastic strain $\bar{\varepsilon}_{\mathrm{p}}$. The relation between yield stress and effective plastic strain can be specified as linear or nonlinear. In the case of linear isotropic hardening, the yield stress is defined as

$$\sigma_y = \sigma_{y0} + \sigma_h(\bar{\varepsilon}_p), \tag{8}$$

where σ_{y0} is the initial yield stress and σ_h is a linear function of the effective plastic strain:

$$\sigma_h(\bar{\varepsilon}_p) = K\bar{\varepsilon}_p, \tag{9}$$

where K is the isotropic hardening modulus, given by

$$\frac{1}{K} = \frac{1}{E_T} - \frac{1}{E}, \tag{10}$$

where E_T and E are the isotropic tangent modulus (stress increment/total strain increment) and Young's modulus, respectively.

FINITE-ELEMENT (FE) MODELING AND NUMERICAL RESULTS

The FE model used is based on the implementation of the thermoelectric equations in the commercial software COMSOL, as described by Bjørk et al.[11] The built-in thermomechanical equations in COMSOL are used to model the mechanical response of the module, assuming elastoplastic material behavior.

Electrothermomechanical Modeling of a TE Module

The system considered in the FE modeling is a 2 × 2 leg thermoelectric (TE) module consisting of *n*-type ($Bi_2Te_{2.85}Se_{0.15}$)[12] and *p*-type (BiSbTe)[13] bismuth telluride legs. The temperature-dependent Seebeck coefficient, electrical resistivity, and thermal conductivity are shown in Fig. 1. The thicknesses of the solder, electrical interconnector, and isolator plate (top and bottom ceramic layers) are 0.1 mm, 0.25 mm, and 0.7 mm, respectively. The hot- and cold-side temperatures of the TE module are taken to be 200°C and 30°C, respectively. Under these operating conditions, the optimized ratio of cross-sectional area of *p*- and *n*-type legs is calculated to be A_p/A_n = 1.17. For simplicity, in the current study, the *p*- and *n*-type cross-sectional areas are considered to be equal (A_p/A_n = 1), as this only results in a very small performance drop,[11] and because this is the aspect ratio often used in commercial modules.

For the thermomechanical analysis of the module, it is assumed that the 2 × 2 TE module is a "building block" of a larger module. Therefore, an elastic foundation is considered for the mechanical boundary condition in the x and y directions. The stiffness of the elastic foundation in the x and y direction is given by

$$K_{x,y} = \frac{E_{Iso}A_{x,y}}{l_{x,y}}, \tag{11}$$

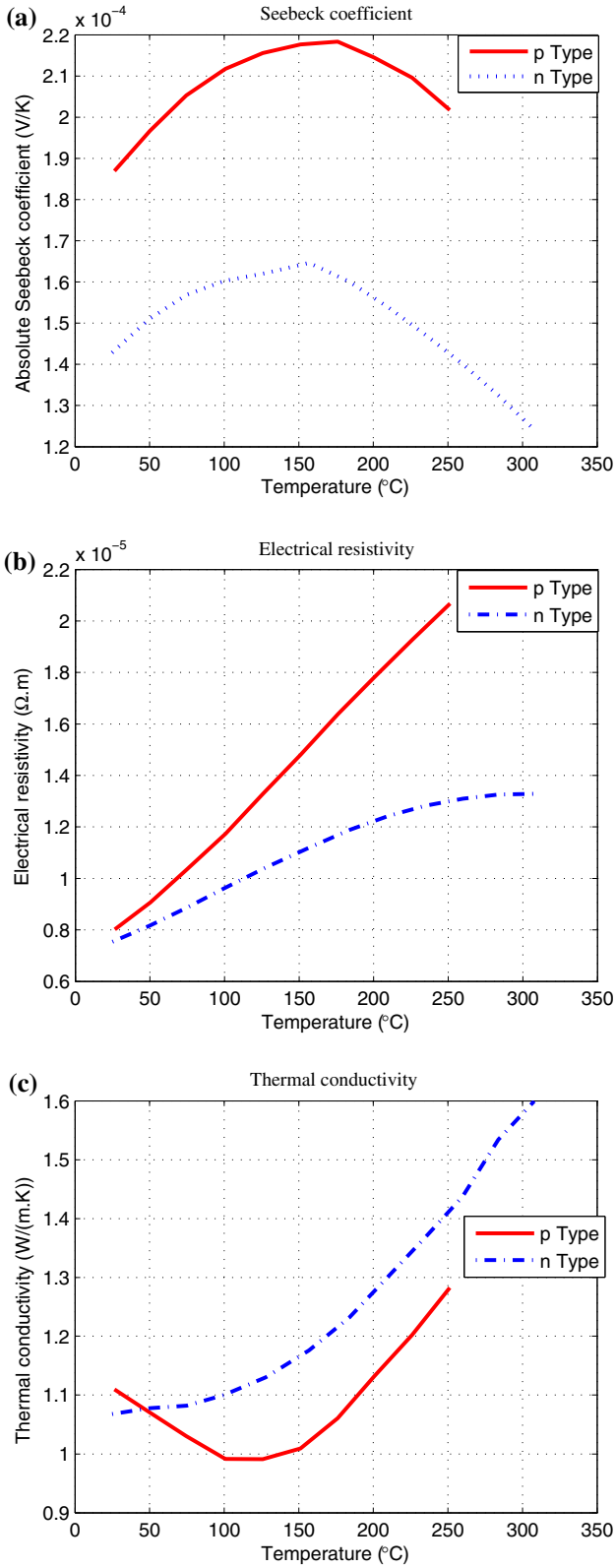

Fig. 1. Thermoelectrical properties of the *n*- and *p*-type bismuth telluride alloys: (a) Seebeck coefficient, (b) electrical resistivity, and (c) thermal conductivity.[12,13]

Table I. Thermal and mechanical properties of the isolator plate, solder, and interconnector[15]

Material	CTE (μm/K)	Thermal Conductivity (W/m-K)	Electrical Conductivity ($\times 10^6$ S/m)	Young's Modulus (GPa)	Poisson's Ratio	Initial Yield Stress (MPa)	Ultimate Tensile Stress (MPa)	Plastic Elongation (%)
Copper interconnector	17.5 ± 5%	395 ± 2%	56 ± 4%	110 ± 1%	0.35 ± 3%	69 ± 1%	221 ± 0.5%	55 ± 2%
Silver interconnector	19.4 ± 2%	413 ± 4%	66 ± 3%	83 ± 1%	0.37 ± 3%	54 ± 2%	125 ± 1%	50 ± 2%
95Sn-5Sb solder	27 ± 3%	28 ± 3%	6.89 ± 0.2%	50 ± 2%	0.33 ± 3%	26 ± 4%	41 ± 2%	38 ± 3%
95Sn-5Ag solder	23 ± 4%	33 ± 3%	7.75 ± 0.1%	56.5 ± 0.2%	0.37 ± 3%	24.8 ± 0.5%	32 ± 3%	49 ± 2%
Alumina substrate	8.1 ± 1%	28 ± 7%	—	300 ± 3%	0.22 ± 4%	–	–	–
p-Type	16.8 ± 1%	See Fig. 1	See Fig. 1	45 ± 2%	0.28 ± 3%	–	–	–
n-Type	16.8 ± 1%	See Fig. 1	See Fig. 1	45 ± 2%	0.28 ± 3%	–	–	–

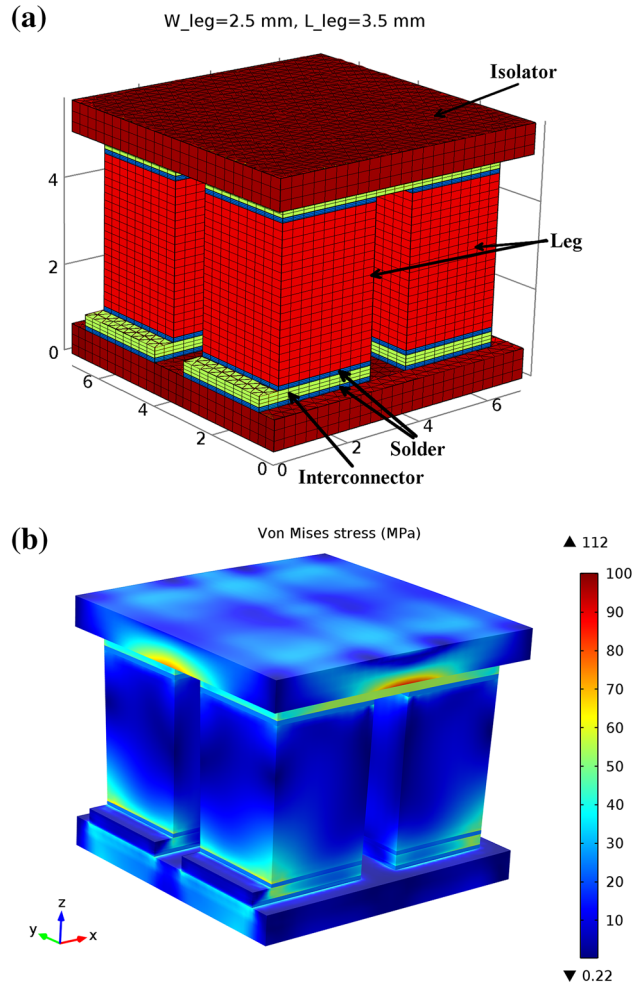

Fig. 2. (a) Initial geometry of the FE model (W = 2.5 mm, L = 3.5 mm); colors indicate different components of the system. (b) Surface plot of von Mises stress in the module.

where E_{Iso}, $A_{x,y}$, and $l_{x,y}$ are the modulus of elasticity, cross-sectional area, and length of the isolator in the x and y direction, respectively.

A load of 150 N/cm^2 is applied on the top plane of the module to simulate good thermal contact, while the vertical component of the displacement is constrained at the bottom plane of the module. The mechanical deformation of the module is simulated using elastoplastic analysis. A bilinear isotropic hardening model is considered for the elastoplastic behavior of the solder–interconnector set.

For each module with different geometrical dimensions, the optimum value of the external resistance is found; i.e., it is always the optimum electrical performance of the module that is reported. Radiative heat transfer between the leg surfaces and ambient is assumed as a heat loss mechanism using the procedure described in detail elsewhere.[11] A value of $\varepsilon = 0.4$ is considered for the emissivity of the bismuth telluride legs. Only the legs are assumed to radiate. The thermal and mechanical properties of the ceramic plate (alumina), interconnectors (copper, silver), and solders are given in Table I. It should be noted that the uncertainties associated with the material properties are naturally reflected in the overall results; however, it was shown that the uncertainty of the figure of merit, ZT, is rather small, estimated to be about ±5% to ±10%.[13,14]

The initial geometry of the FE model and surface plot of the von Mises stress are depicted in Fig. 2 for leg dimensions of 2.5 mm width and 3.5 mm length. For this module, the maximum thermal stresses in the legs are at the edges at the cold side (Fig. 2b). This is because the plastic deformation of the solder in the vicinity of the hot side diminishes the stress at this side. This was observed to be the case for modules with larger width ($W \geq 2.5$ mm) due to the considerable plastic deformation of the solder at the hot side. Figure 3 shows surface plots of the temperature and electrical potential in the module.

The geometrical dimensions of the legs, i.e., their length and width, were varied from 0.5 mm to 4.5 mm with a step size of 1 mm. The output power, efficiency, and induced thermal stresses were calculated for each of these dimensions. The distance

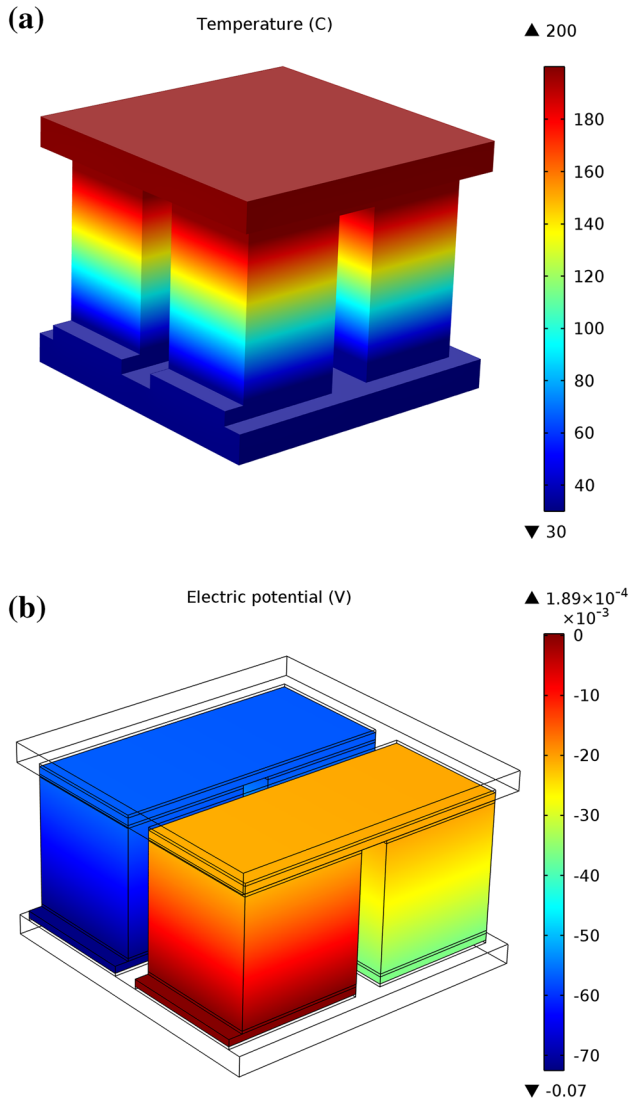

Fig. 3. Surface plots of (a) temperature and (b) electrical potential.

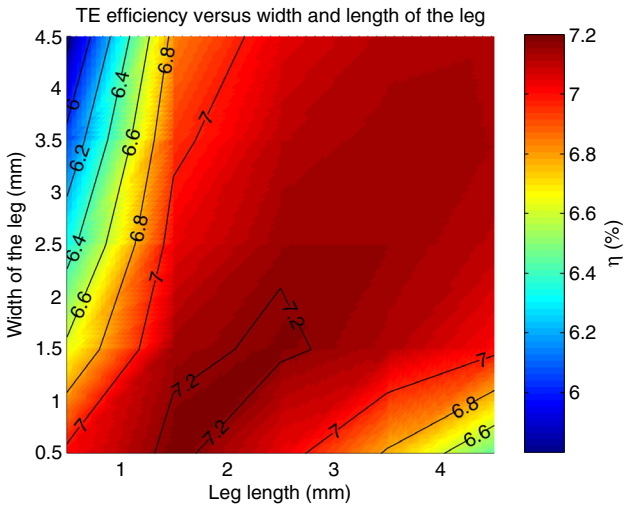

Fig. 4. Contour plot of TE efficiency versus length and width of legs.

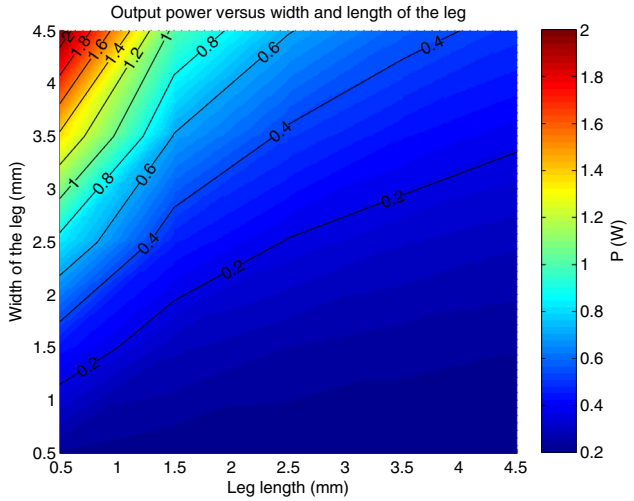

Fig. 5. Contour plot of TE output power versus length and width of legs.

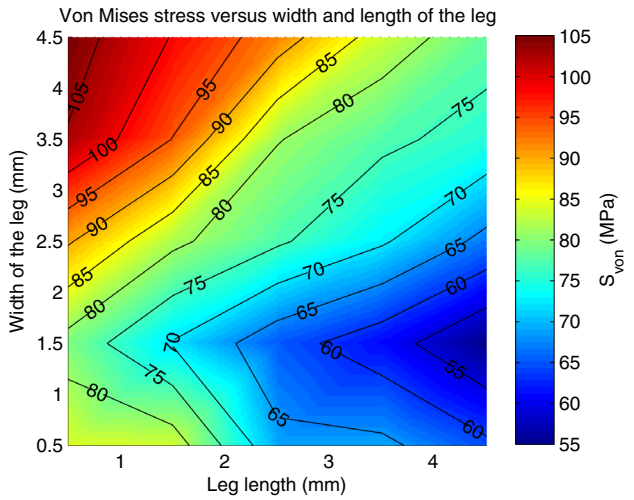

Fig. 6. Contour plot of maximum von Mises stress in the legs versus their length and width.

between the legs was kept constant at 1 mm. The side edges of the isolator plate are at a distance of 1 mm from the outer edges of the legs. Figures 4, 5, and 6 depict contour plots of the efficiency, output power, and maximum von Mises stress in the legs as a function of their length and width.

As can be seen from Fig. 4, the thermoelectric efficiency for constant leg width increases with increasing leg length until a certain level, after which it declines. As seen from Table II, the thermal resistance of the legs constitutes the major part of the module thermal resistance. Therefore, increasing the leg length increases the overall thermal resistance of the module considerably, and consequently the temperature difference between the cold and hot sides of the leg (Fig. 7), hence the efficiency rises. The increase in the temperature difference with leg length is due to the fact that the thermal

Table II. Thermal resistance of different components of the TE module for W = 1.5 mm

	Thermal resistance (m^2-K/W)				
Component	***L*_leg = 0.5 mm**	***L*_leg = 1.5 mm**	***L*_leg = 2.5 mm**	***L*_leg = 3.5 mm**	***L*_leg = 4.5 mm**
Alumina plate	1.73	1.73	1.73	1.73	1.73
Silver interconnector	0.10	0.10	0.10	0.10	0.10
95Sn-5Ag solder	1.17	1.17	1.17	1.17	1.17
Legs	52.9	158.7	264.5	370.4	476.2
Module	55.9	161.7	267.5	373.4	479.2

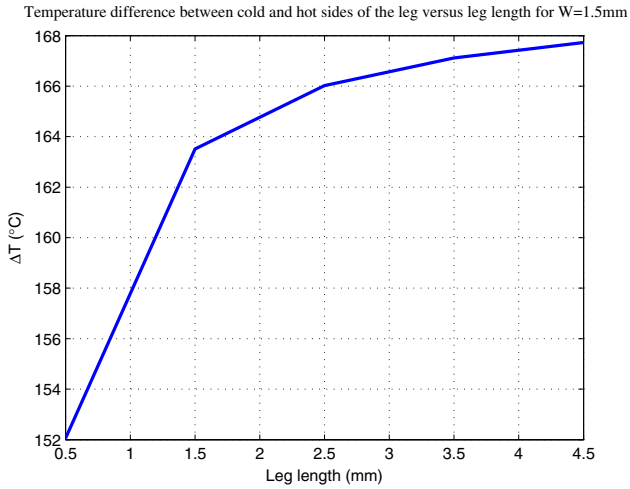

Fig. 7. Increase in temperature difference between cold and hot sides of the leg with increase in leg length.

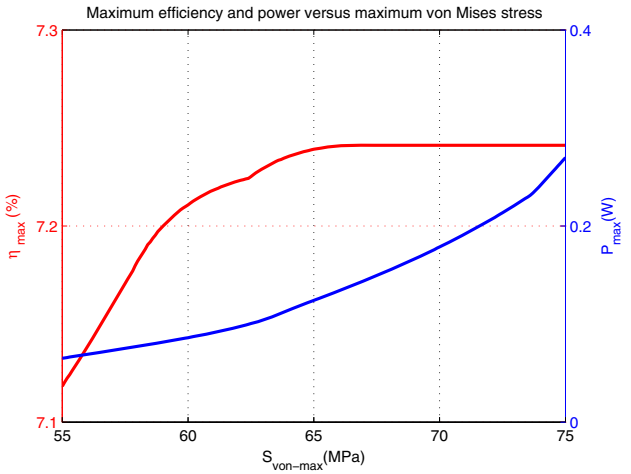

Fig. 8. Maximum efficiency and maximum output power versus maximum von Mises stress.

resistance of the insulator, solder, and electrical interconnector is constant (Table II), thus increasing the thermal resistance of the leg decreases the temperature drop associated with these components. The decrease in efficiency is due to increase of the radiative heat loss from the legs, as the surface area increases. The adverse effect of the radiative heat loss on the efficiency is more obvious for the modules with smaller cross-sectional area of the legs. This is because, the thinner the leg, the higher their surface area to volume ratio (A/V), hence the radiative heat loss from the surfaces increases.

As expected, the output power is directly and inversely proportional to the width and length of the legs, respectively (Fig. 5).

Figure 6 illustrates that legs with larger cross-sectional area experience higher thermal stresses, while the opposite applies for longer legs. However, there is one exception for the increase of the width of the legs (Fig. 6) when the solder deforms transiently from the elastic to plastic regime (when the width of the leg increases in the range of 0.5 mm to 1.5 mm). The plastic deformation at the solder–leg, solder–interconnector, and solder–isolator interfaces reduces the thermal expansion mismatch between the different layers, hence decreasing the thermal stresses induced in the module. Therefore, proper selection of the width of the leg could reduce the induced thermal stresses in the legs significantly.

To obtain an optimized design, the length of the legs should be, on the one hand, long to gain the maximum efficiency and minimum thermal stresses, but on the other hand, short enough to produce high output power (Figs. 4–6). If the von Mises stress is constrained by a maximum value of 75 MPa (i.e., $S_{\text{von\_max}} \leq 75\text{MPa}$), the maximum efficiency and output power versus the maximum von Mises stress can be plotted as shown in Fig. 8. Accordingly, the ranges of geometrical dimensions of the leg at maximum efficiency and power are obtained as

For maximum efficiency: 2 mm $< L_{\text{leg}} <$ 2.5 mm, 1.5 mm $< W_{\text{leg}} <$ 2 mm

For maximum power: 1 mm $< L_{\text{leg}} <$ 1.5 mm, 1.5 mm $< W_{\text{leg}} <$ 2 mm

This can provide a guideline for optimizing the geometrical dimensions of the legs for maximum

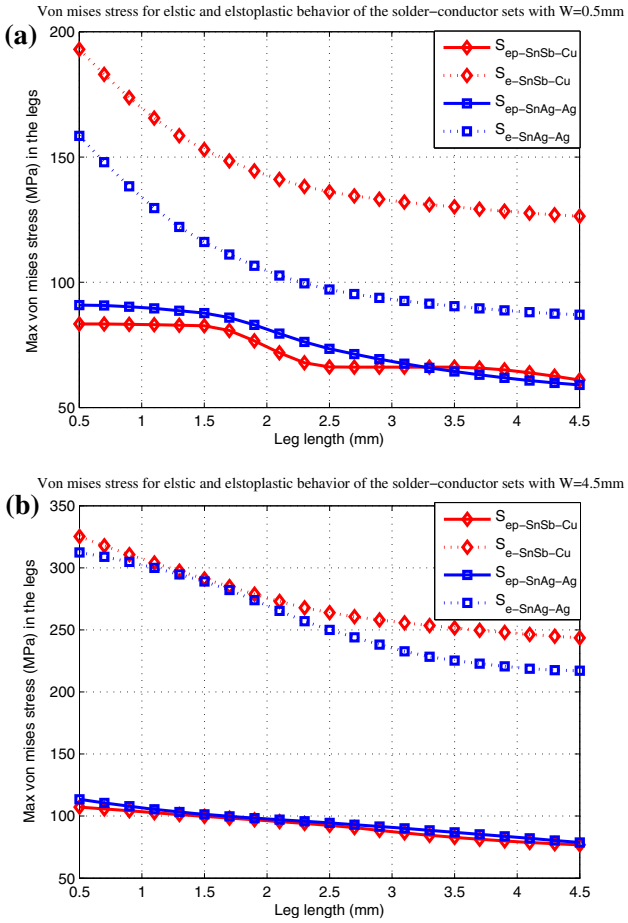

Fig. 9. Maximum von Mises stress in the legs for both elastic and elastoplastic behavior of the interconnector/solder set: (a) $W = 0.5$ mm and (b) $W = 4.5$ mm.

efficiency and output power, subject to a constraint on the induced thermal stresses.

Effect of Different Solders and Interconnector Materials as Well as the Corresponding Mechanical Models

In this part of the study, the effect of solders and interconnector materials on the thermal stresses developed in the module for two different sets of solder/interconnector materials, namely 95Sn-5Sb/Cu and 95Sn-5Ag/Ag, is evaluated. These solder/interconnector sets are suitable for the low–medium temperature range of bismuth telluride TE modules. Besides the elastoplastic calculations described above, a simple elastic approximation was also used. Even though the elastic model is computationally much less intensive and has been used in previous works,[2–4] it predicts wrong thermal stresses for some thermal and mechanical boundary conditions, especially when some components (solder and interconnector) of the module undergo considerable plastic deformation. To evaluate this error, both elastic and elastoplastic analyses were used for modeling the mechanical behavior of the solder/interconnector sets, to evaluate the importance of taking into account the plastic deformation of these components.

Figure 9 depicts the maximum von Mises stress in the legs for the two different solder/interconnector sets, namely 95Sn-5Sb/Cu and 95Sn-5Ag/Ag, when considering different mechanical behavior (elastic and elastoplastic) for the sets. From Table I, it can be noticed that the thermal expansion mismatch at the solder/leg, solder/interconnector, and solder/isolator pairs is higher for the module with 95Sn-5Sb/Cu than that for its counterpart with 95Sn-5Ag/Ag. Hence, higher thermal stress is expected in the module with 95Sn5Sb-Cu compared with its counterpart. This is valid when the developed stresses are in the elastic range of the solder/interconnector set, but once the stress exceeds the elastic range, the plastic deformation of the solder or both the solder and interconnector (at high thermal stresses) causes significant stress relaxation and inverts this condition (Fig. 9). In other words, the higher the plastic deformation, the higher the stress relaxation. As seen from Fig. 9, in the case of the elastic behavior assumption for the interconnector/solder set, the thermal stress induced in the module with 95Sn-5Sb/Cu is greater than for its counterpart, while this is almost the other way around when the elastoplastic behavior of the solder/interconnector set is taken into account. Therefore, in the elastic range, the magnitude of the stress in the module and accordingly the mechanical reliability is dependent on the thermal expansion mismatch between the constituent materials, however once the solder or interconnector undergoes plastic deformation, the mechanism and magnitude of the plastic deformation plays an important role in the stress magnitude and accordingly the mechanical reliability.

CONCLUSIONS

In the present study, thermoelectromechanical modeling of a TE module made of n- and p-type bismuth telluride alloys was carried out, and the output power, efficiency, and thermal stresses induced in the module were calculated for different geometrical dimensions. Furthermore, the influence of the solder and interconnector materials as well as their mechanical behavior on the thermal stresses induced in the legs was assessed. The results reveal that increasing the length of the legs reduces the output power and the thermal stresses in the module, while the efficiency decreases or increases depending on the width of the legs, or more precisely their area to volume ratio. In addition, increasing the width of the legs leads to an increase in the thermal stresses (if the plastic limit is reached) as well as the output power. Based on these results, it is suggested that the length of the legs should be, on the one hand, long enough to produce the maximum efficiency and minimum

thermal stresses, but on the other hand, short enough to keep the output power at a high level. Moreover, the width of the legs should be large enough to produce high output power, and at the same time small to keep the thermal stresses low. As a guideline, for the condition that the legs are constrained to maximum von Mises stress of 75 MPa, for maximum efficiency the leg length should be 2 mm to 2.5 mm and the leg width 1.5 mm to 2 mm, while for maximum power, the leg length should be 1 mm to 1.5 mm and the leg width 1.5 mm to 2 mm.

It was also shown that the transition from elastic to plastic deformation in the solder/interconnector set decreases the developed thermal stresses considerably. Comparison of the thermal stresses in a module with two different solder/interconnector sets, namely 95Sn-5Sb/Cu and 95Sn-5Ag/Ag, shows that, in the elastic range, the magnitude of the stress is proportional to the thermal expansion mismatch between the different constituent materials, while beyond the elastic limit the stress magnitude is highly dependent on the magnitude and mechanism of the plastic deformation in the module.

Finally, these results provide a basis for designing and optimizing TE modules for maximum output power and efficiency as well as minimum thermal stresses. Design optimization for a TE module under cyclic loading is proposed for future work.

ACKNOWLEDGEMENTS

The authors would like to thank the Programme Commission for Energy and Environment (EnMi), The Danish Research and Innovations (Project No. 10-093971) for sponsoring the OTE-POWER research work as well as supporting the CTEC project.

REFERENCES

1. P.H. Ngan, D.V. Christensen, G.J. Snyder, L.T. Hung, S. Linderoth, N. Van Nong, and N. Pryds, *Phys. Status Solidi* 211, 9 (2014).
2. E. Suhir and A. Shakouri, *J. Appl. Mech.* 80, 021012 (2012).
3. E. Suhir and A. Shakouri, *J. Appl. Mech.* 79, 061010 (2012).
4. A. Ziabari, E. Suhir, and A. Shakouri, *Microelectron. J.* 45, 547 (2014).
5. T. Clin, S. Turenne, D. Vasilevskiy, and R.A. Masut, *J. Electron. Mater.* 38, 994 (2009).
6. J.-L. Gao, Q.-G. Du, X.-D. Zhang, and X.-Q. Jiang, *J. Electron. Mater.* 40, 884 (2011).
7. M. Picard, S. Turenne, D. Vasilevskiy, and R.A. Masut, *J. Electron. Mater.* 42, 2343 (2013).
8. J.C. Simo and T.J.R. Hughes, *Computational Inelasticity* (New York: Springer, 1998), pp. 71–151.
9. M.-H. Yu, G.-W. Ma, H.-F. Qiang, and Y.-Q. Zhang, *Generalized Plasticity* (Berlin: Springer, 2006), pp. 122–153.
10. J. Chakrabarty, *Applied Plasticity,* ed. F.F. Ling, 2nd edn. (Boston, MA: Springer, 2010), pp. 1–48.
11. R. Bjørk, D.V. Christensen, D. Eriksen, and N. Pryds, *Int. J. Therm. Sci.* 85, 12 (2014).
12. H.L. Ni, X.B. Zhao, T.J. Zhu, X.H. Ji, and J.P. Tu, *J. Alloys Compd.* 397, 317 (2005).
13. Y. Ma, Q. Hao, B. Poudel, Y. Lan, B. Yu, D. Wang, G. Chen, and Z. Ren, *Nano Lett.* 8, 2580 (2008).
14. W.J. Xie, J. He, S. Zhu, X.L. Su, S.Y. Wang, T. Holgate, J.W. Graff, V. Ponnambalam, S.J. Poon, X.F. Tang, Q.J. Zhang, and T.M. Tritt, *Acta Mater.* 58, 4705 (2010).
15. ASM International Handbook Committee, *Metals Handbook, Vol.2*: *Properties and Selection: Nonferrous Alloys and Special-Purpose Materials*, 10th edn. (ASM International, Materials Park, 1990).